UMR DEPARTMENT OF MECHANICAL & AEROSPACE ENGINEERING

FINAL TECHNICAL REPORT

AERODYNAMIC-STRUCTURAL ANALYSIS OF DUAL BLADED HELICOPTER SYSTEMS

NASA AMES NSG-2375

BY

BRUCE P. SELBERG

DONALD L. CRONIN

KAMRAN ROKHSAZ

JOHN R. DYKMAN

CARLA J. YAGER

FEBRUARY 1980

UNIVERSITY OF MISSOURI - ROLLA

AERODYNAMIC-STRUCTURAL ANALYSIS OF DUAL BLADED HELICOPTER SYSTEMS

Aerodynamic Analysis

Bruce P. Selberg
Associate Professor

Kamran Rokhsaz
Graduate Research Assistant

Structural Analysis

Donald L. Cronin
Professor

John R. Dykman
Research Assistant

Carla J. Yager
Research Assistant

February 1980

Department of Mechanical and Aerospace Engineering

University of Missouri-Rolla

Rolla, MO 65401

THIS DOCUMENT SHOULD NOT BE CONSIDERED AS AN OPEN PUBLICATION IN THAT IT CONTAINS PROPRIETARY INFORMATION THAT HAS BEEN FILED IN A PATENT DISCLOSURE

SUMMARY

The aerodynamic analysis indicated significant power savings for the birotor over the monorotor for St = 1.0, Ga = 0.26 and either De = -4 degrees or De = -6 degrees. These savings occured for all three rotor radii at De = -6 degrees and for the seventeen and twenty feet radii at De = -4 degrees. When these results are considered with the structural analysis which indicates that for both the seventeen and fourteen feet cases, where the birotor and monorotor are of equal weights, the birotor deflections are of the same general magnitude as the monorotor with one tip connection between the birotor blades. The tip connection is required because of the uneven loads on the upper and lower rotors and the sensitivity of the aerodynamics to decalage angle and gap.

A more optimized structural system in which the blade weight is reduced might move the blade radius of the birotor closer to 14 feet case. In this area the birotor would weigh less while still exhibiting the improved aerodynamics for St = 1.0, Ga = 0.26, and De = -6 degrees. While it is realized that the enclosed analysis has not achieved the optimal aerodynamic structural birotor configuration it has demonstrated birotor feasibility in that the birotor system can operate with substantial required power savings with no weight penalty or with substantial weight savings for the same required power as the single rotor.

AERODYNAMIC SUMMARY

An analytical study was undertaken to assess the aerodynamic feasibility of the birotor blade concept. The study investigated:

1. Inviscid flow field about dual bladed rotor.
2. Boundary layer separation on the rotors.
3. Three dimensional induced drag calculations.
4. Rotor thrust and power required.

The aerodynamic study led to the following conclusions:

1. The best aerodynamic results for the dual rotor occurred for a blade stagger of one chord length, a blade gap of twenty six percent of the chord length, and an angle of attack between the two blades of -6 degrees.
2. For blade placement; i.e. stagger -St, gap -Ga, and decalage angle -De, that gave the improved aerodynamic results, the boundary layer separated further back on the dual blades than for the single bladed rotor.
3. The delayed separation over the dual bladed rotor systems results in a lower pressure and viscous drag than for the single blade.
4. The induced drag and, hence, induced torque is lower for the dual rotor system than the single rotor system when decalage angles are -4 and -6 degrees.
5. The dual rotor at a Ga = 0.26, St = 1.0, and De = -6 degrees requires significantly lower power levels than the single rotor. The dual rotor at the same gap and stagger, but with De = -4 degrees, also requires lower power levels.
6. The dual rotor at a Ga = 0.33, St = 1.0, De = -4 degrees and -6 degrees requires lower power levels than the single rotor.
7. As a result of the lift of the upper and lower dual rotors being different and the sensitivity of the results to proper gap and decalage angles, it will be necessary to tie the two rotors together at the tips with a possible addition tie at the position of the second bending moment.

AERODYNAMIC-STRUCTURAL ANALYSIS OF DUAL BLADED HELICOPTER SYSTEMS

An aerodynamic-structural analysis was carried out for dual bladed and single bladed helicopter rotor systems. A typical birotor configuration, as it would be mounted, is shown in figure 1. The upper and lower blades maintain this same position relative to one another as they rotate. An end view of the blades are shown in figure 2. The distance one blade is ahead of the other is called stagger in percent of chord, St, with a positive stagger indicating the upper blade is forward of the lower blade. The gap, in percent of chord, is designated Ga. The angle of attack between the two blades is called decalage angle, De, and is negative when the extended chord lines intersect in front of the two blade elements. The aerodynamic structural analysis considered the hover mode of operation and all dual bladed systems were chosen to have the same lifting area as the single bladed system. In addition aspect ratio of the single bladed rotor was selected as 20 and each aerodynamic birotor blade was selected such that they had the same aspect ratio as the single rotor. Three different diameter birotor combinations were chosen to assess aerodynamic and structural performance, 28, 37, and 40 feet in diameter. A constant chord NACA 0012 airfoil section with an 8 degree linear twist was selected for all calculations. The blades had an airfoil section form 0.25R to R where R is the blade radius from the hub of rotation. Rotor tip velocity for all cases was 600 feet per second. The blade sizes along with the mode of operation are shown in Table 1.

AERODYNAMIC ANALYSIS

The analysis level can most easily be discussed with respect to four main areas which are listed below:

1. Inviscid flow field analysis to investigate aerodynamic characteristics for various dual rotor blade placement combinations with respect to blade stagger, gap, and angle of attack between the two blades.
2. Boundary layer separation point analysis and subsequent viscous and pressure drag analysis.
3. Induced drag calculation for the three dimensional dual and single rotor system.
4. Compilation and integration of the above to predict thrust and power requirements.

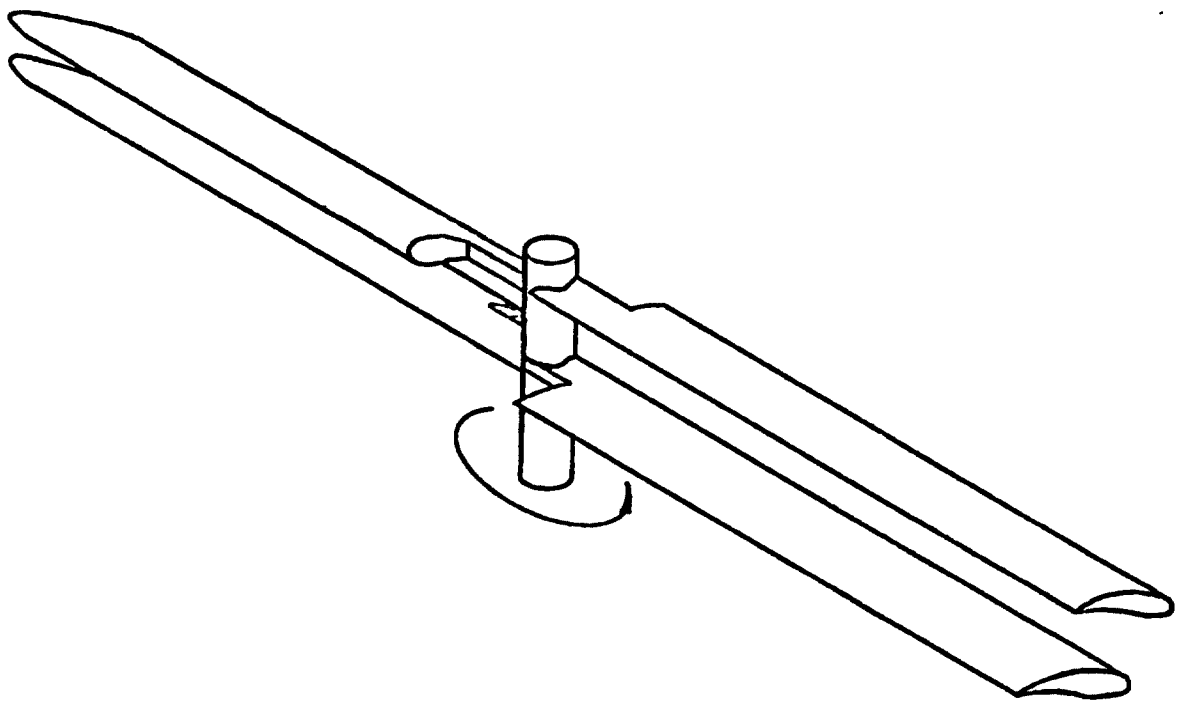

Figure 1

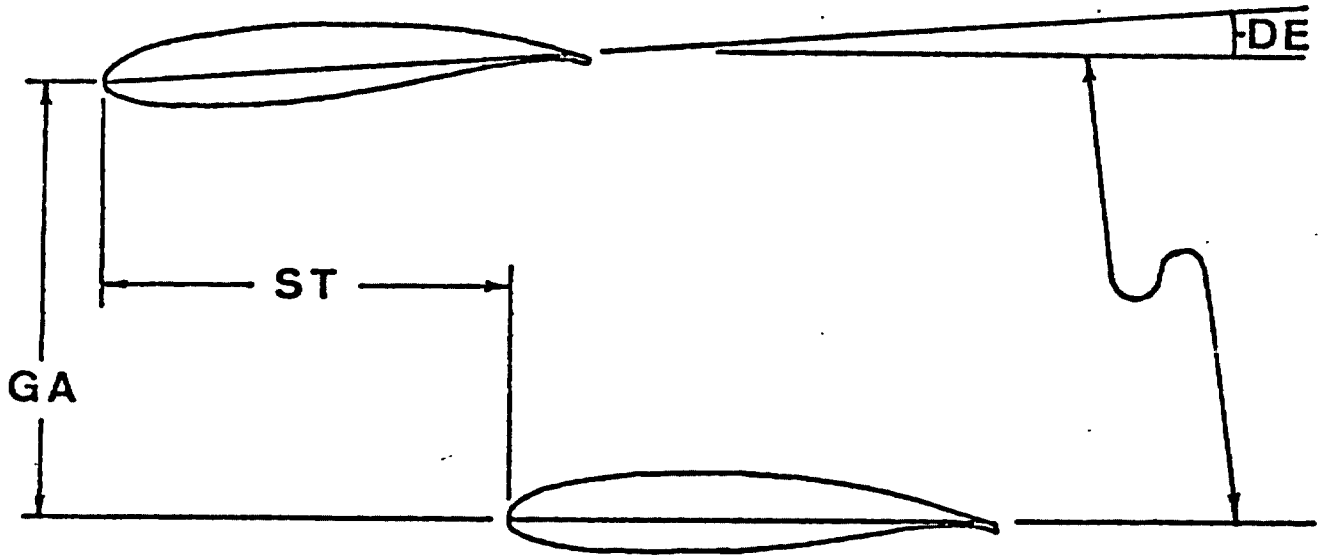

Figure 2

TABLE 1

AIRFOIL CHARACTERISTICS

NACA 0012, constant chord blade
8 degree linear twist from 0.25R to R
Rotor tip speed - 600 feet per second

Single rotor blade dimensions
diameter = 40 feet
chord = 2 feet

Dual rotor blade dimensions
Case I
diameter = 28 feet
chord = 1.415 feet
Case II
diameter = 37 feet
chord = 1.175 feet
Case III
diameter = 40 feet
chord = 1.0 foot

Inviscid Analysis

Nenadovitch[1] who did extensive computations and tests with two element airfoils obtained aerodynamic improvements for the two element case over the single element case only in a narrow range of St, Ga, and De. This region was when St ≈ 1.0, Ga ≈ .33 to .66, and De = -3 to -6 degrees. For gaps greater than one, negative staggers, or for positive decalage angles the two element aerodynamic characteristics were degraded with respect to the single element.

Laplace's equation of the stream function was solved using a finite difference approach in a Cartesian coordinate system. Pressure distribution results for the NACA 0012 airfoil section were compared with those of Raj[2], Eppler[3], and G. Krabedian[4] to validate the numerical technique with agreement being excellent.

The inviscid computational analysis was carried out in this narrow region of St, Ga, and De where Neadovitch found aerodynamic improvements. Figure 3 is the pressure coefficient, Cp, distribution for the upper and lower elements for a St = 1.0, Ga = 0.26, and De = -4 degrees for the lower airfoil at a geometric angle of attack

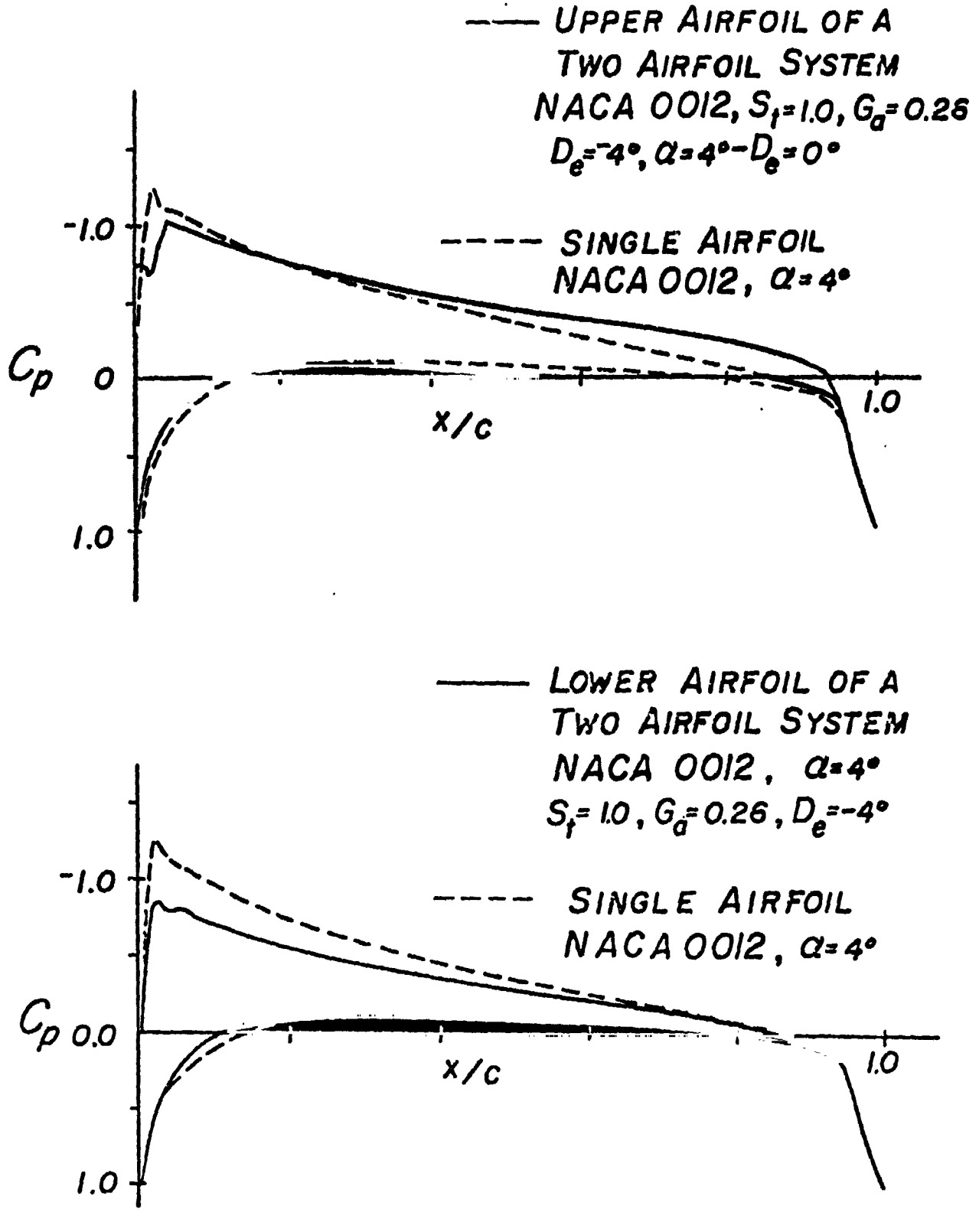
UPPER AIRFOIL OF A
TWO AIRFOIL SYSTEM
NACA 0012, S_t=1.0, G_a=0.26
D_e=-4°, α=4°-D_e=0°
SINGLE AIRFOIL
NACA 0012, α=4°
-1.0
C_p 0
1.0
x/c
1.0
LOWER AIRFOIL OF A
TWO AIRFOIL SYSTEM
NACA 0012, α=4°
S_t= 1.0, G_a=0.26, D_e=-4°
SINGLE AIRFOIL
NACA 0012, α=4°
-1.0
C_p 0.0
1.0
x/c
1.0

Figure 3

of 4 degrees. Superimposed is the pressure distribution for a single airfoil element at 4 degree geometric angle of attack. Even though the upper airfoil is at a zero geometric angle of attack with respect to the freestream velocity vector it has a pressure distribution and hence a lift that corresponds to approximately 4 degree angle of attack. The resulting lift vector on the upper airfoil is thus rotated giving an effective thrust or negative drag with respect to the direction of motion. The lower airfoil has a Cp distribution slightly less than the 4 degree single airfoil case. The net result for the combined two elements is small changes in total lift coefficient along with a negative induced two dimensional drag coefficient, $C_{D_{2i}}$. At an 8 degree geometric angle of attack a similar distribution is shown in figure 4. Again the upper airfoil, due to the flow interaction, is acting like a single airfoil at a angle of attack greater than 8 degree even though the geometric angle of attack is only 4 degrees. Although the lower airfoil has a Cp distribution corresponding only to a four degree angle of attack the total lift coefficient stays nearly the same while the induced two dimensional drag coefficient $C_{D_{2i}}$ is significant and beneficial. Figure 5 shows the induced two dimensional drag coefficient as a function of lift coefficient for different decalage angles. Both the -4 and -6 degree decalage cases demonstrate good improvements at all angles of attack while the De = -2 degree case only gives a negative induced drag at low lift coefficients. Figure 6 illustrates the effect of gap for the -4 and -6 degree decalage cases. Both decalage cases demonstrate that the highest negative induced drag coefficient levels are obtained for the narrowest gap investigated with improvements falling off as the gap increases. Gaps of less than 0.26 could not be obtained because the submatrix of each wing's flow field would overlap causing numerical computational problems. For the De = -4 degree case at Ga = 0.26 the effects of stagger were investigated. These are shown in figure 7. Again the St = 1.0 case demonstrates the best results.

Boundary Analysis and Separation

A separation and viscous flow analysis after E. Truckenbrodt[5] was used to predict separation points and the viscous drag over the single and dual element cases. Figure 8 shows separation points results on the upper surface of the upper airfoil as a function of x/c and De in comparison with the single rotor. For St = 1.0, and Ga = 0.26 the single rotor separates before the birotor in all instances. The lower rotor does not have any significant separation over either its upper or lower surface and is not shown. The separation problems which do happen for the single rotor occur when $C_l \geq 0.6$. Thus the differences between the birotor and single rotor will be more pronounced for blades with either a larger geometric twist than 8 degrees or for

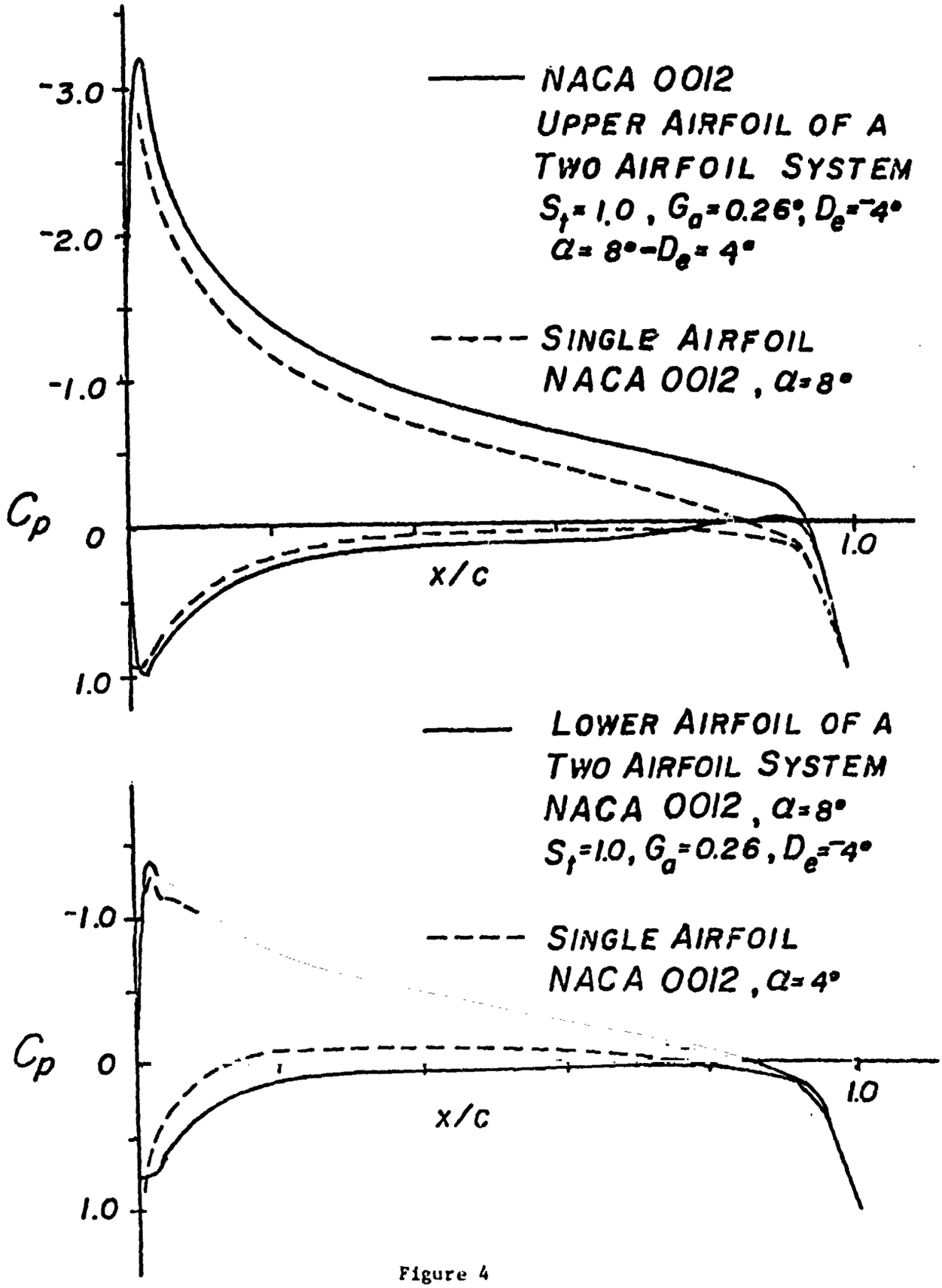
NACA 0012
UPPER AIRFOIL OF A
TWO AIRFOIL SYSTEM
$S_t = 1.0$, $G_a = 0.26$; $D_e = -4°$
$\alpha = 8° - D_e = 4°$
SINGLE AIRFOIL
NACA 0012, $\alpha = 8°$
-3.0
-2.0
-1.0
C_p
0
1.0
x/c
1.0
LOWER AIRFOIL OF A
TWO AIRFOIL SYSTEM
NACA 0012, $\alpha = 8°$
$S_t = 1.0$, $G_a = 0.26$, $D_e = -4°$
SINGLE AIRFOIL
NACA 0012, $\alpha = 4°$
-1.0
C_p
0
1.0
x/c
1.0

Figure 4

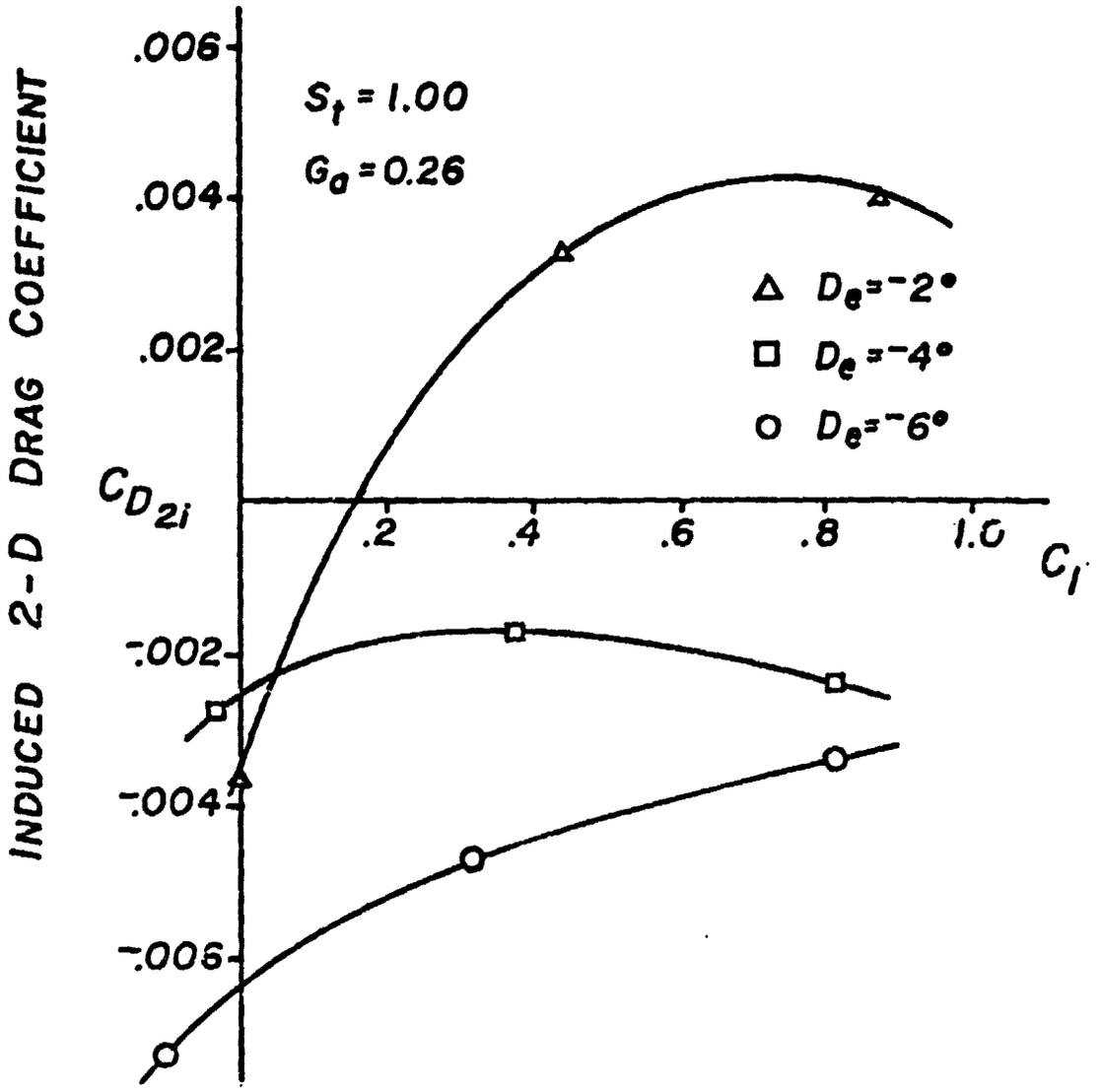
INDUCED 2-D DRAG COEFFICIENT
$C_{D_{2i}}$
.006
.004
.002
-.002
-.004
-.006
$S_t = 1.00$
$G_a = 0.26$
$D_e = -2°$
$D_e = -4°$
$D_e = -6°$
.2
.4
.6
.8
1.0
C_l

Figure 5

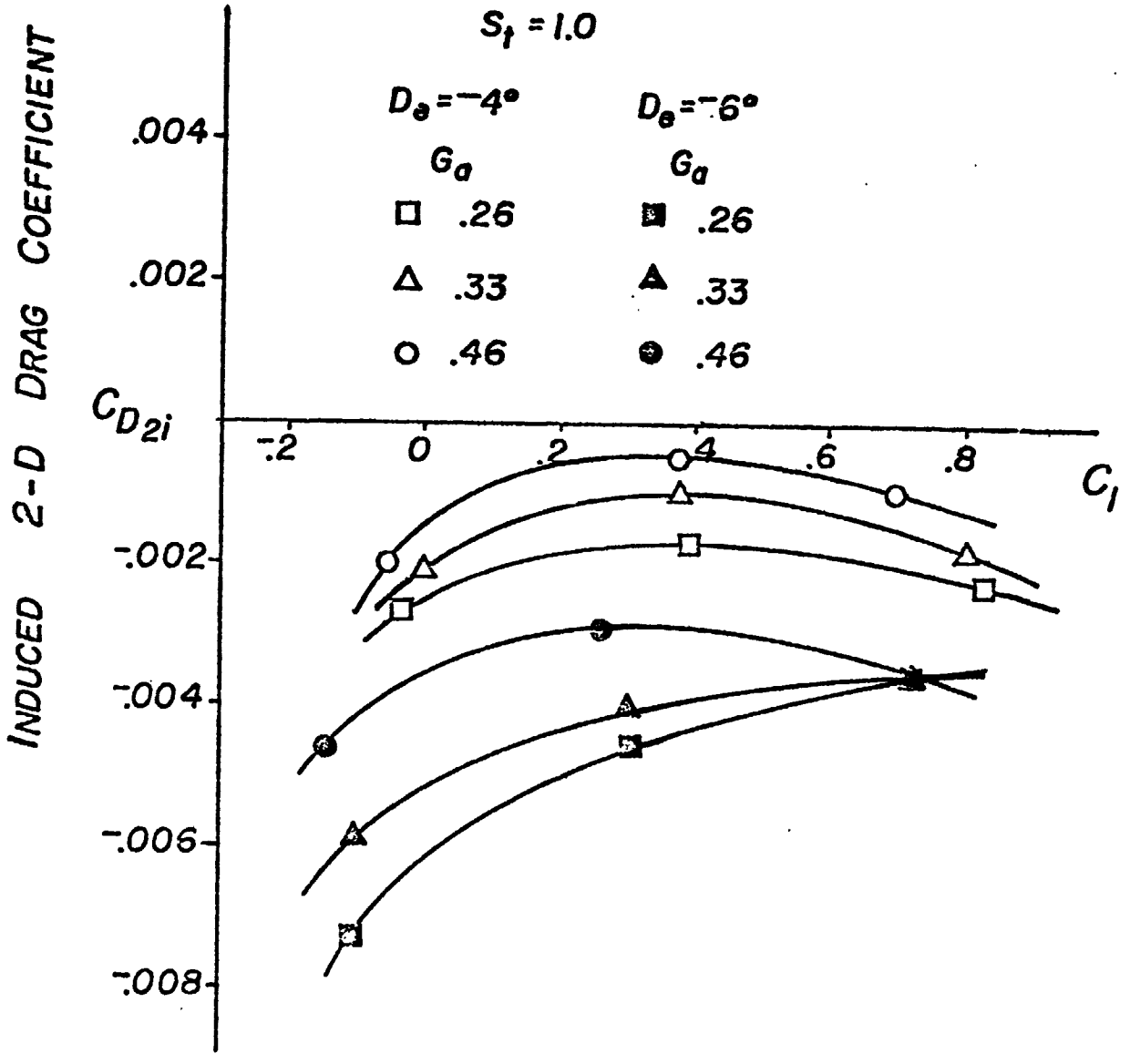
$S_t = 1.0$
$D_e = -4°$
$D_e = -6°$
G_a
G_a
.26
.33
.46
.26
.33
.46
.004
.002
-.002
-.004
-.006
-.008
$C_{D_{2i}}$
INDUCED 2-D DRAG COEFFICIENT
-.2
0
.2
.4
.6
.8
C_l

Figure 6

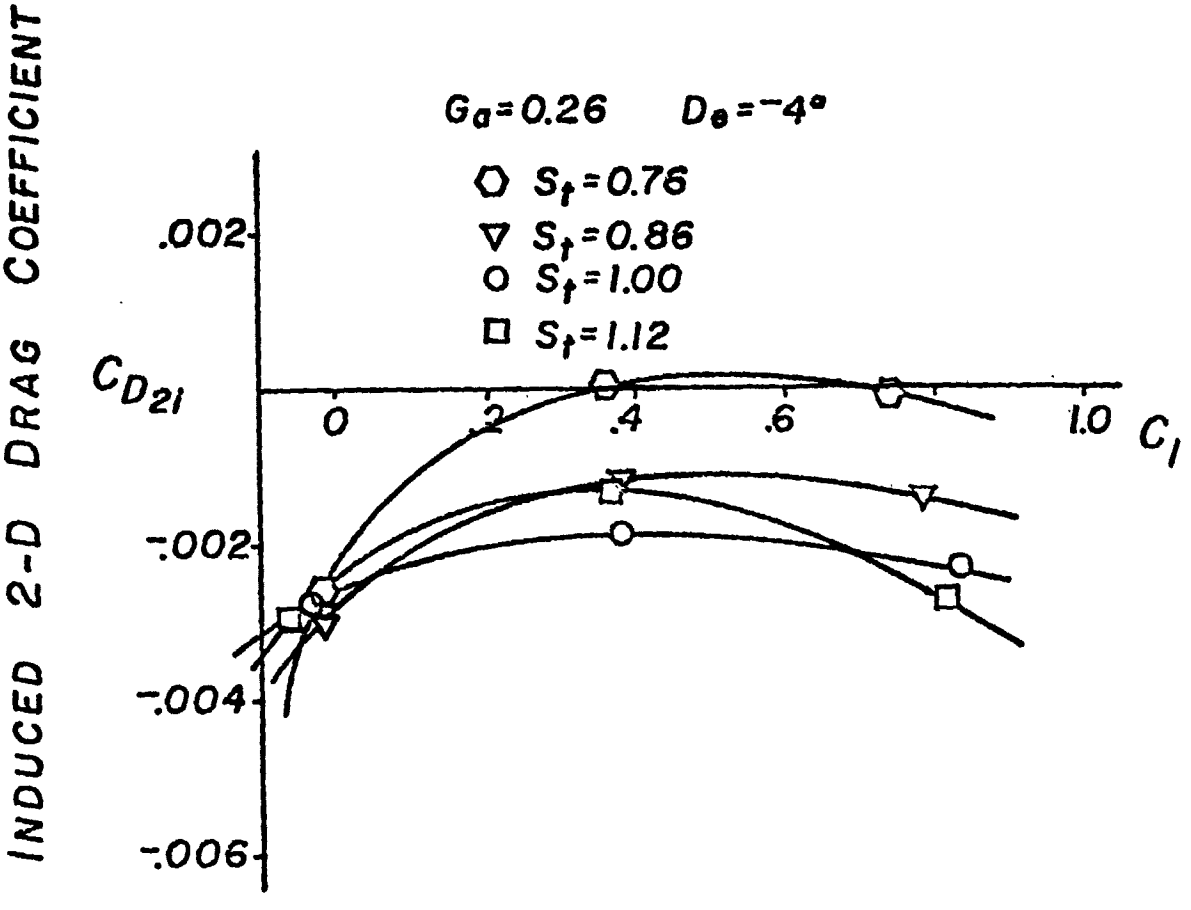
INDUCED 2-D DRAG COEFFICIENT
$C_{D_{2I}}$
$G_a = 0.26$ $D_e = -4°$
$S_t = 0.76$
$S_t = 0.86$
$S_t = 1.00$
$S_t = 1.12$
.002
-.002
-.004
-.006
0
.2
.4
.6
1.0
C_l

Figure 7

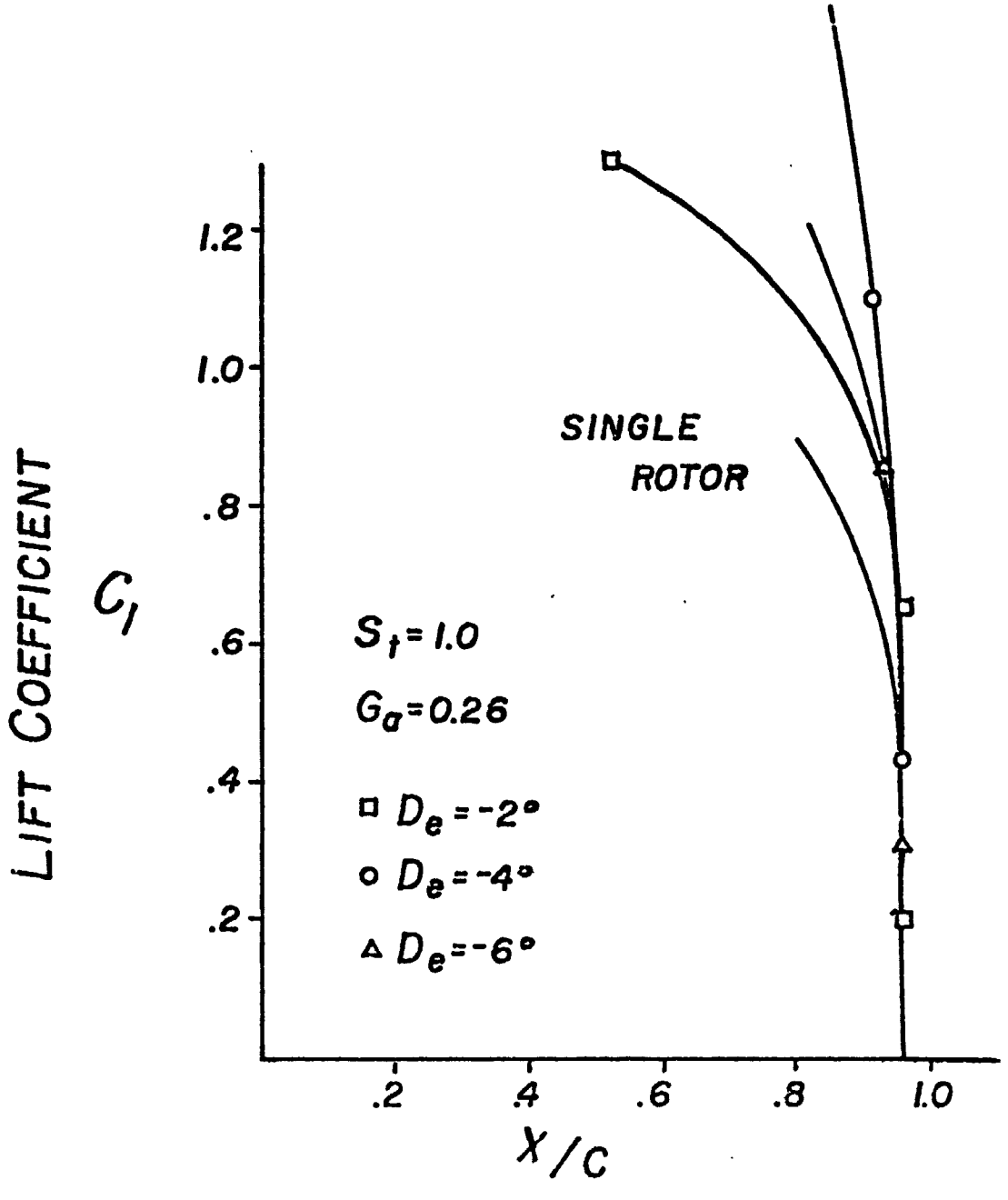
LIFT COEFFICIENT
C_l
1.2
1.0
.8
.6
.4
.2
SINGLE
ROTOR
$S_t = 1.0$
$G_a = 0.26$
$D_e = -2°$
$D_e = -4°$
$D_e = -6°$
.2
.4
.6
.8
1.0
X/C

Figure 8

the 8 degree case considered but at higher angles of attack, i.e. from 12 degrees to 4 degrees instead of from 8 degrees to 0 degrees or 9 degrees to 1 degree as considered herein. The birotor is not separating significantly even for C_l as high as 1.2 for St = 1.0, De = -4 degrees and -6 degrees and for all gaps considered. Figure 9 shows that as gap increases the birotor moves in the direction of the single rotor although not rapidly. Figure 10 shows the effect of stagger. Except for St = 0.76 the separation point does not demonstrate any trends or move significantly.

It was anticipated that viscous and pressure drag after separation would be calculated. However, due to computational problems in predicting the pressure drag after separation, the viscous and pressure drag were obtained from two dimensional data for a single rotor at the same C_l. Thus the benefits from the later separation on the birotor do not appear in these final thrust-power required curves. When these corrections are applied, the birotor will have even lower power required results and higher lift results than those reported herein.

Three Dimensional Induced Drag

Finite aspect ratio rotor induced drag calculations were made using the classical vortex filament analysis. This analysis was applied between 0.25R and R since the analysis is symmetric with respect to the hub. Figure 11 shows induced torque results for a St = 1.0, Ga = 0.26 as a function of decalage angle and rotor radius. Except for the -2 degrees decalage angle the induced torque for the birotor is less than the single rotor. While variations due to rotor radius are small there is a significant variation in induced torque with respect to decalage angle with the -6 degree decalage angle having the least induced torque. Some of the induced torque that occurs as the decalage angle gets more negative is probably due to the lower rotor lift that exits at these decalage angles.

Thrust and Power

When the sectional C_l's are integrated over R, as well as the sectional values of $C_{D_{2i}}$, $C_{D_{viscous}}$, $C_{D_{induced}}$ we get thrust and required power. Figure 12 shows the required power versus thrust as a function of decalage angle at a St = 1.0 and a Ga = 0.26 for the three birotor and monorotor radii. As would have been expected from the previous results, the De = -2 degrees case requires birotor power that is essentially the same as that of the monorotor. However the -4 degrees and -6 degrees decalage cases show significantly lower required power levels than for the single rotor case. When the -6 degrees decalage angle results are linearally extrapolated to

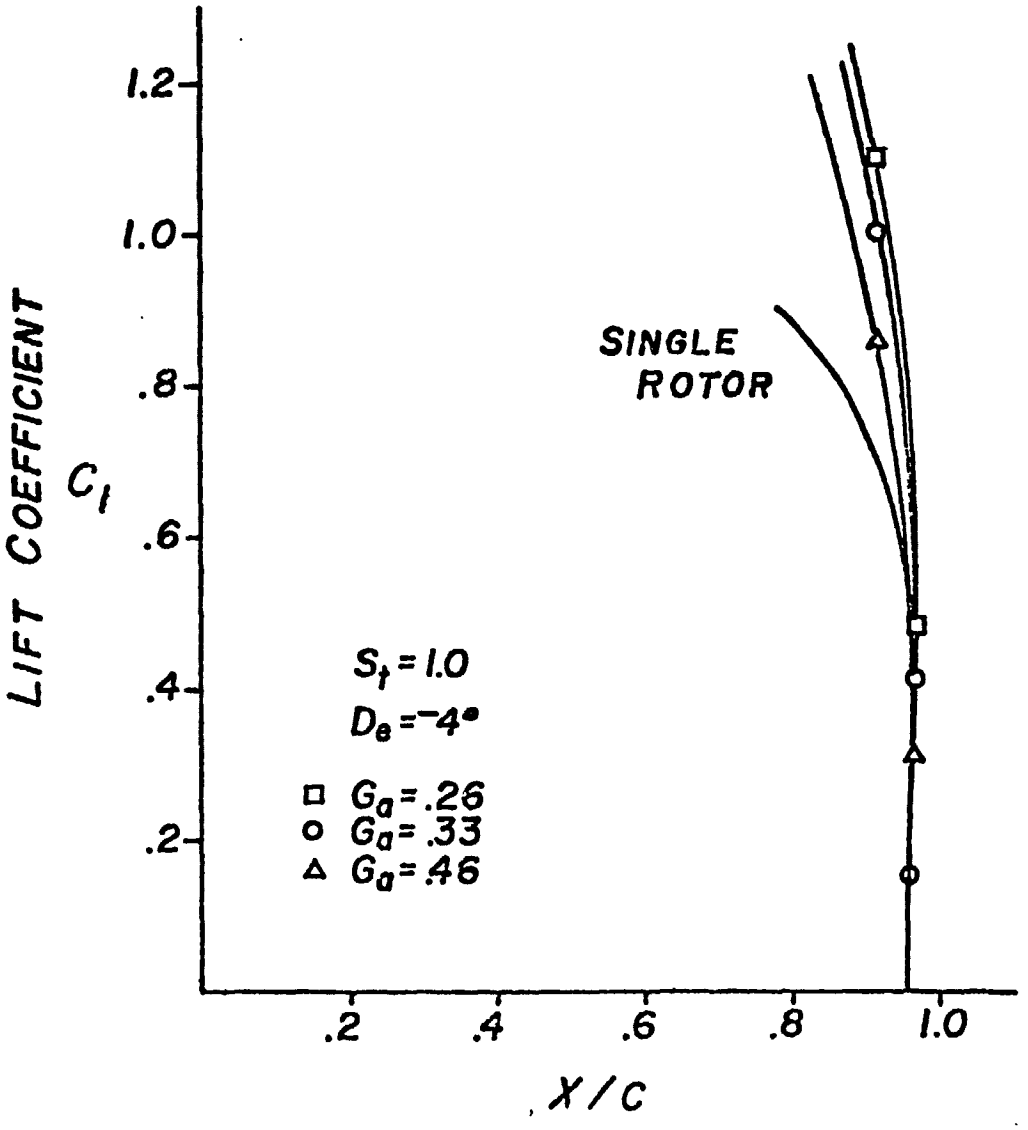
LIFT COEFFICIENT
C_l
1.2
1.0
.8
.6
.4
.2
SINGLE ROTOR
$S_t = 1.0$
$D_e = -4°$
$G_a = .26$
$G_a = .33$
$G_a = .46$
.2
.4
.6
.8
1.0
X/C

Figure 9

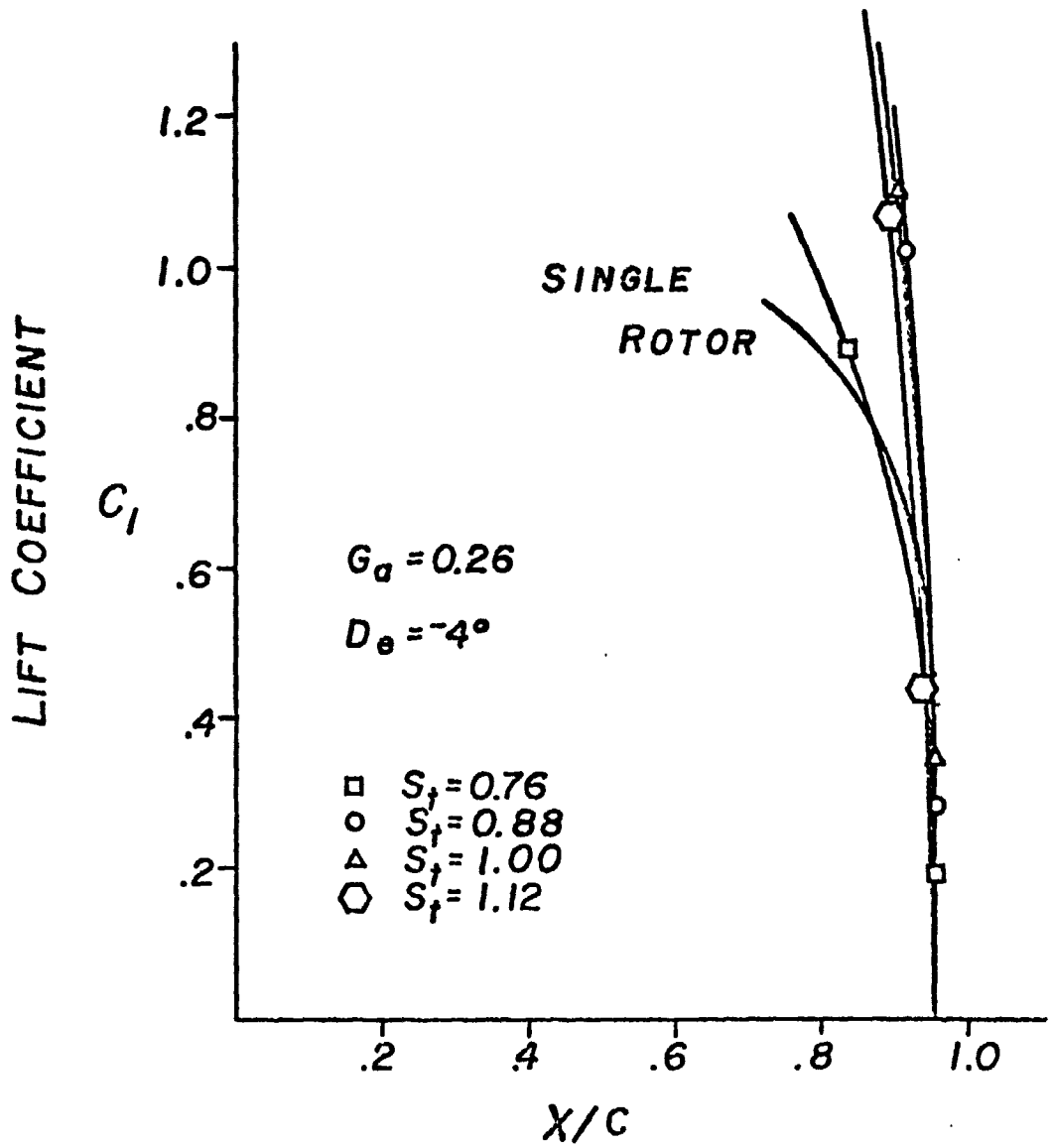
LIFT COEFFICIENT
C_l
1.2
1.0
.8
.6
.4
.2
SINGLE
ROTOR
$G_a = 0.26$
$D_\theta = -4°$
$S_t = 0.76$
$S_t = 0.88$
$S_t = 1.00$
$S_t = 1.12$
.2
.4
.6
.8
1.0
X/C

Figure 10

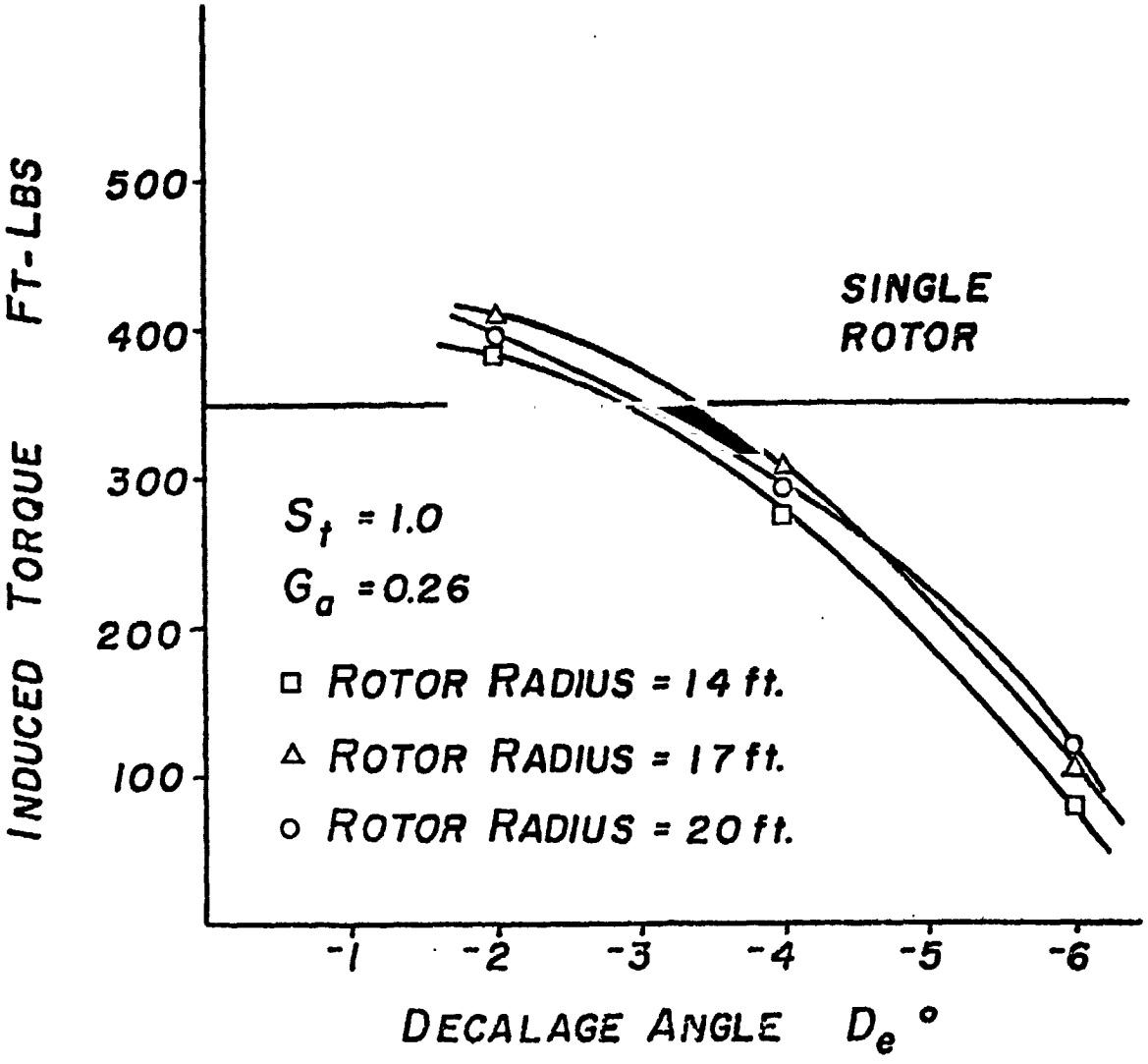
INDUCED TORQUE FT-LBS
500
400
300
200
100
SINGLE ROTOR
S_t = 1.0
G_a = 0.26
□ ROTOR RADIUS = 14 ft.
△ ROTOR RADIUS = 17 ft.
○ ROTOR RADIUS = 20 ft.
-1
-2
-3
-4
-5
-6
DECALAGE ANGLE D_e °

Figure 11

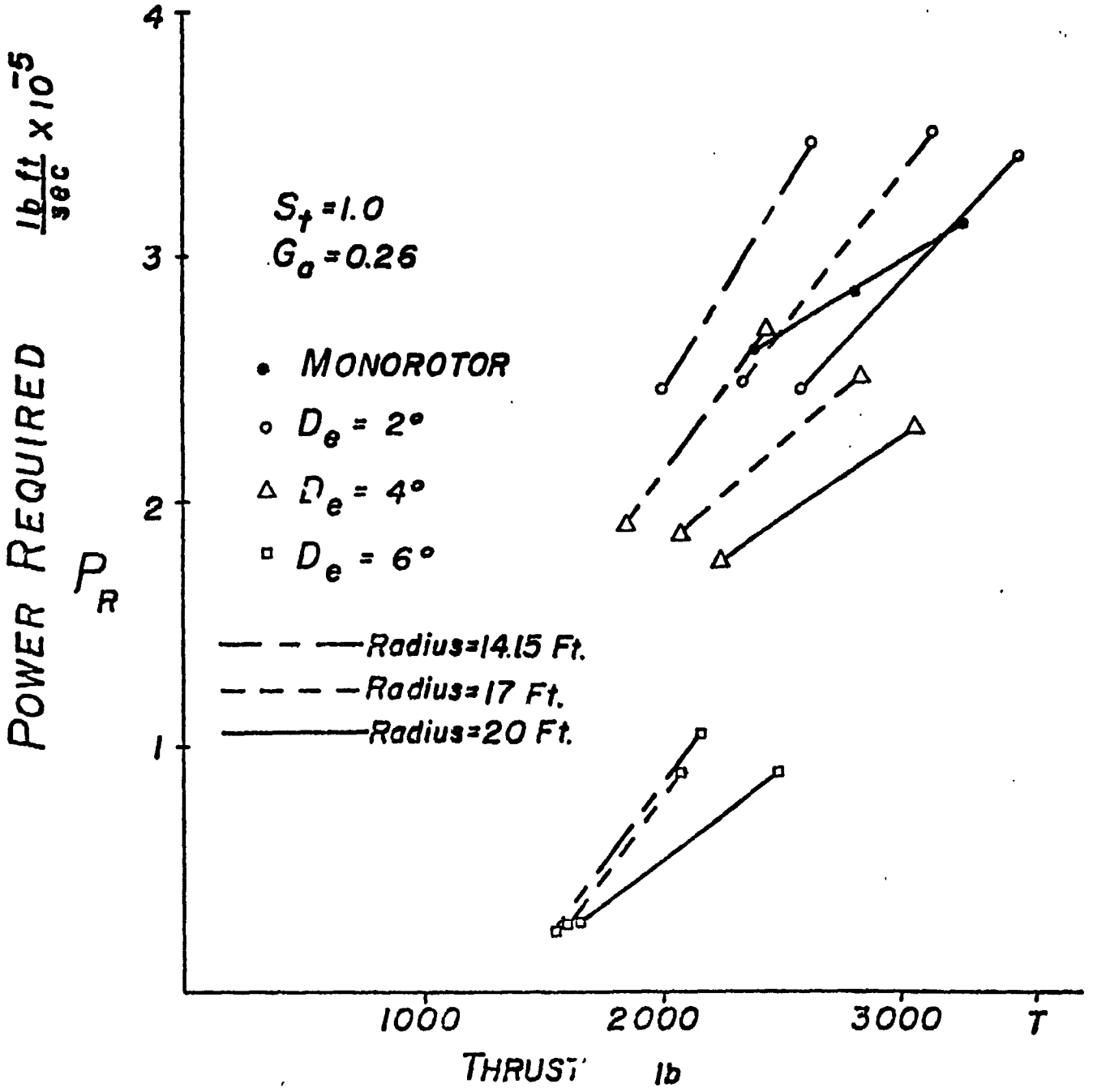
POWER REQUIRED P_R $\frac{lb\,ft}{sec} \times 10^{-5}$
4
3
2
1
$S_t = 1.0$
$G_a = 0.26$
• MONOROTOR
○ $D_e = 2°$
△ $D_e = 4°$
□ $D_e = 6°$
— — — Radius=14.15 Ft.
— — — Radius=17 Ft.
——— Radius=20 Ft.
1000
2000
3000
T
THRUST lb

Figure 12

the same thrust levels as those of the single rotor the required power levels are still significantly below those of the single rotor. This is true for all three birotor radii considered. In figure 13 the same power required thrust curve are shown except for a Ga = 0.33. The same general trends occurs as for the Ga = 0.26 case except the required power levels are slightly higher for the birotor cases. Figure 14 again illustrates power required versus thrust trends except for a Ga = 0.46. However, except for the -6 degrees decalage case the required power levels are of the same or higher than the single rotor. A linear extrapolation of the -6 degrees results yields lower required power only for the 40 feet and 34 feet diameter blades. In figure 15 the results for stagger are shown. For a Ga = 0.26 and De = -4 degrees the stagger is varied from 0.76 to 1.12. The St = 1.0 yields the best results followed by St = 1.12, St = 0.88, and finally St = 0.76.

Due to the sensitivity of the required power results to both gap and decalage angle it is necessary that spacers attach the upper and lower rotor together. This is required because the upper and lower rotors are carrying significantly different loads when the rotors are positioned for the best power required results. The structural analysis indicates that with one tie at the tip of the rotor blades the change in decalage angle is insignificant while the change in gap is acceptable for the 17 foot rotor blades. Two ties, one at the tip and the other at the second bending moment produced insignificant changes in both gap and decalage angle. The added drag these ties would cause can be minimized by covering the tie with an airfoil section that is free to rotate and align itself with the incoming flow.

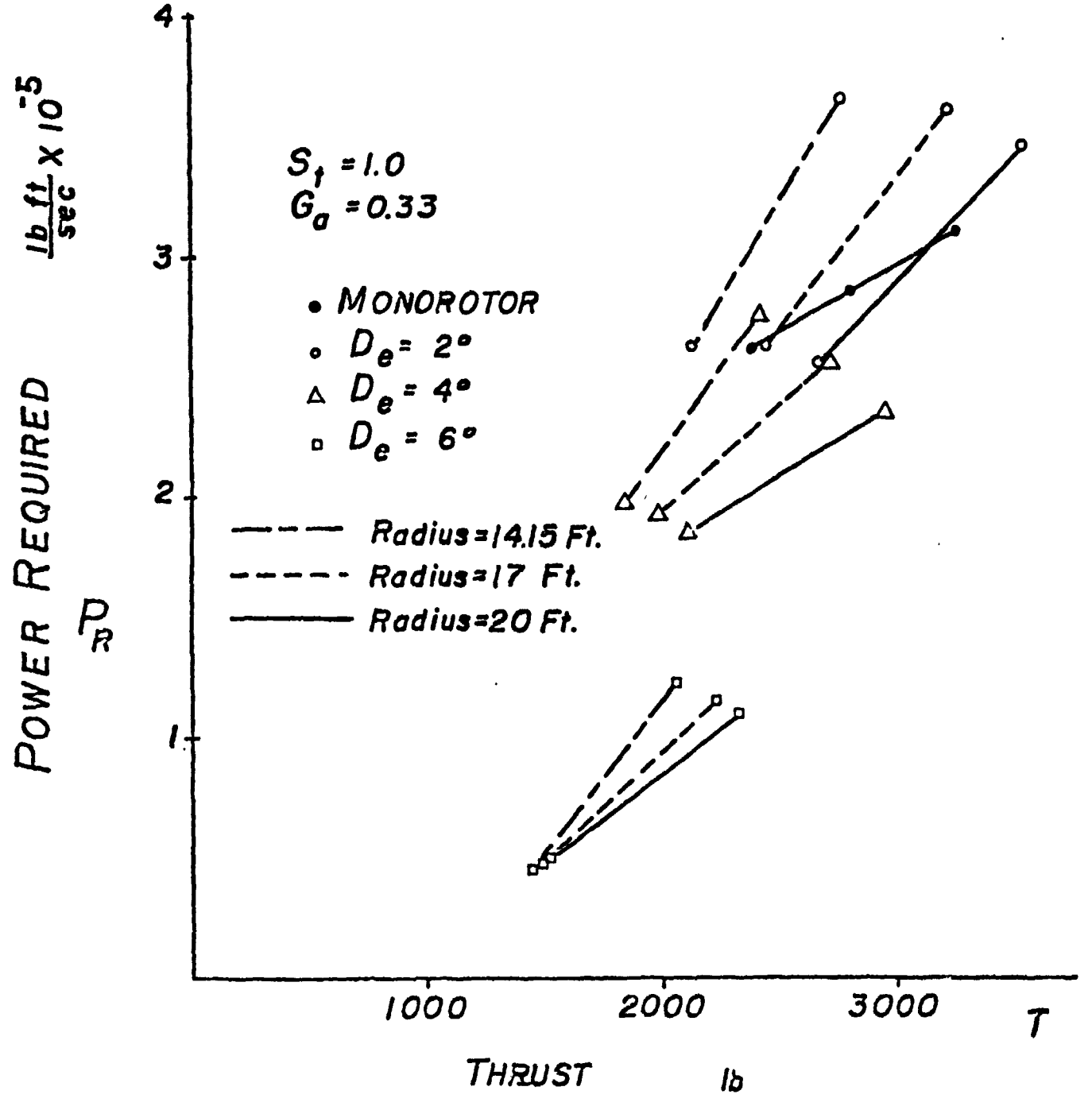
POWER REQUIRED P_R
$\frac{lb\ ft}{sec} \times 10^{-5}$
4
3
2
1
$S_t = 1.0$
$G_a = 0.33$
• MONOROTOR
○ $D_e = 2°$
△ $D_e = 4°$
□ $D_e = 6°$
Radius=14.15 Ft.
Radius=17 Ft.
Radius=20 Ft.
1000
2000
3000
T
THRUST lb

Figure 13

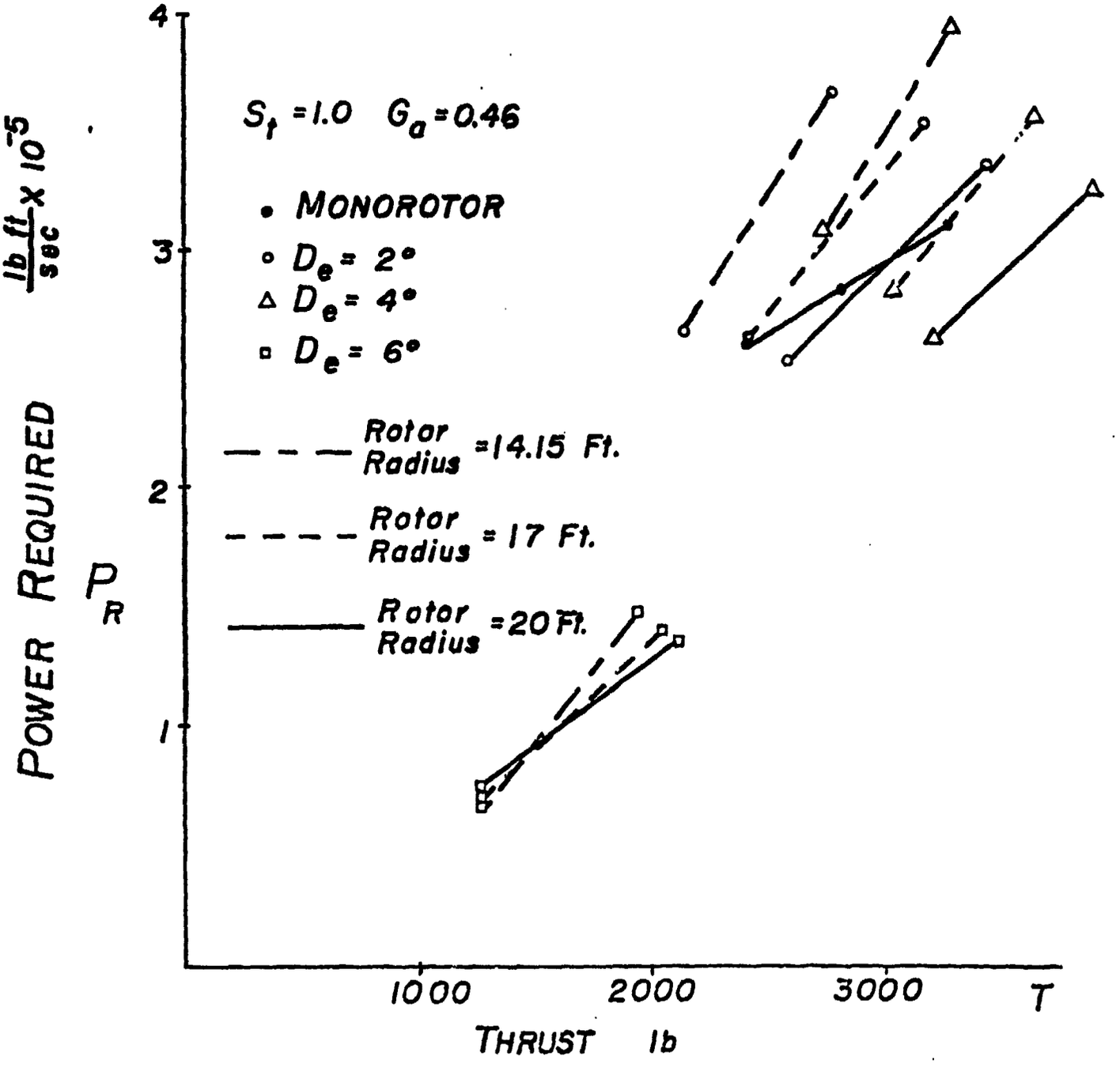
POWER REQUIRED P_R $\frac{lb\ ft}{sec} \times 10^{-5}$
4
3
2
1
$S_f = 1.0$ $G_a = 0.46$
• MONOROTOR
○ $D_e = 2°$
△ $D_e = 4°$
□ $D_e = 6°$
Rotor Radius = 14.15 Ft.
Rotor Radius = 17 Ft.
Rotor Radius = 20 Ft.
1000
2000
3000
T
THRUST lb

Figure 14

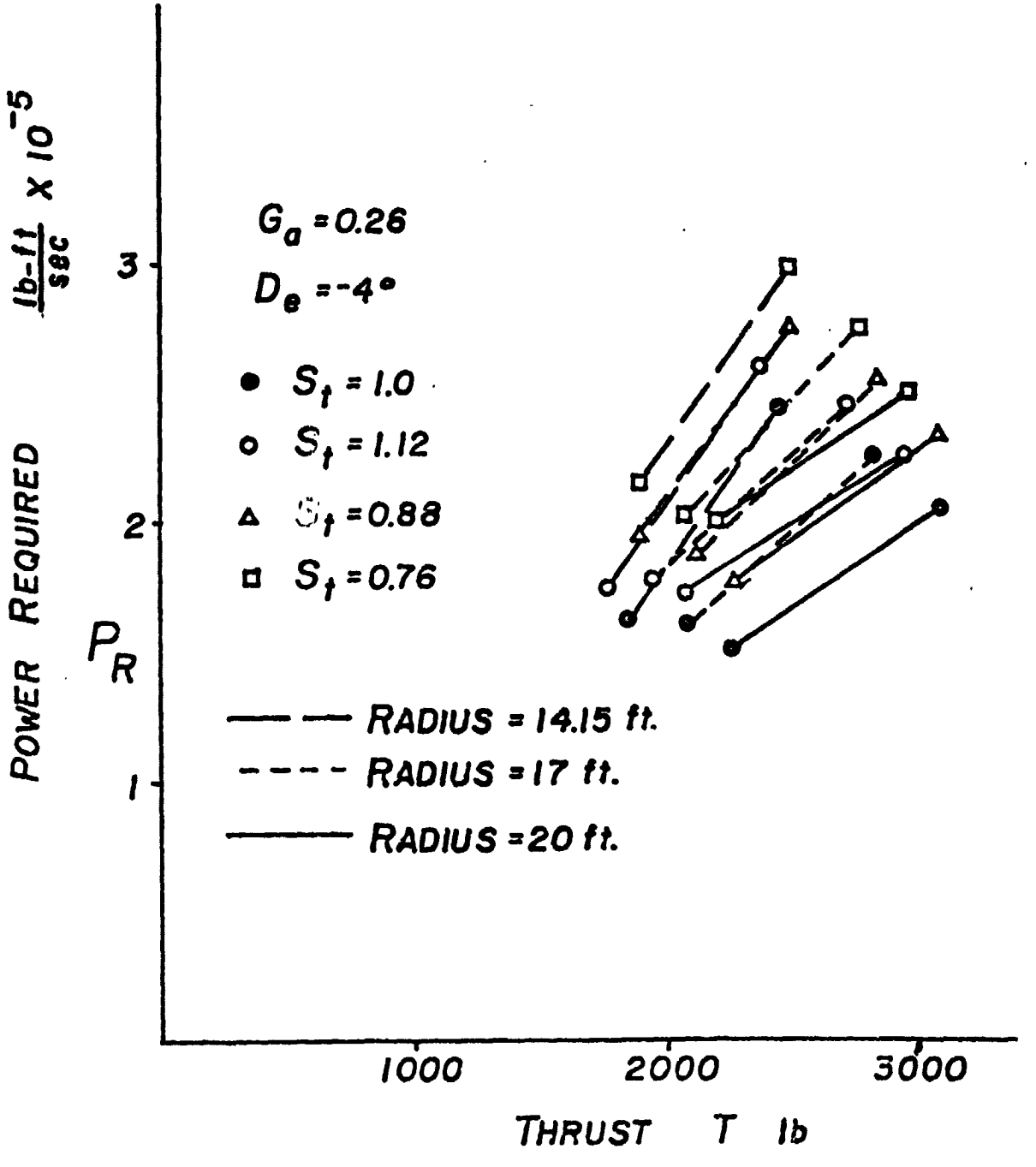
POWER REQUIRED $\frac{lb\text{-}ft}{sec} \times 10^{-5}$
P_R
3
2
1
$G_a = 0.26$
$D_e = -4°$
$S_t = 1.0$
$S_t = 1.12$
$S_t = 0.88$
$S_t = 0.76$
RADIUS = 14.15 ft.
RADIUS = 17 ft.
RADIUS = 20 ft.
1000
2000
3000
THRUST T lb

Figure 15

STRUCTURAL SUMMARY

An analytical study was undertaken to assess the structural feasibility of the birotor helicopter blade concept.

The study focused on two aspects of structural performance:

1. Response of a representative birotor to loading characterizing a steady-state hover.
2. Natural frequencies of a representative birotor.

In order to evaluate birotor structural performance, birotor behavior was compared to that of a baseline single blade. Criteria for birotor structural feasibility included:

1. Blade stresses for the birotor do not exceed values consistent with current aerospace practice as exemplified by stresses in the baseline blade.
2. Hub loads produced by the birotor do not exceed values consistent with current aerospace practice as exemplified by loads produced by the baseline blade.
3. Significant natural frequencies of the birotor fall generally in the neighborhood of significant natural frequencies of the baseline blade.

The study led to the following conclusions:

1. The birotor is in theory a dynamically balanced configuration. True balance may, therefore, be achieved by the addition of small correction weights. Stability and control problems for this configuration are, therefore, not anticipated.
2. The birotor without structural spacers between blades is not a feasible configuration. One spacer connecting blade tips produces acceptable structural performance and may be acceptable aerodynamically. Two spacers -- one connecting blade tips and one connecting blades near the second in-plane bending antinode -- lead to deflections in steady-state hover which are acceptable from the aerodynamic standpoint.

STRUCTURAL ANALYSIS

Modeling Effort

NASTRAN was employed as the primary modeling tool for this study. At study initiation, various models were tested against analytical results to obtain a model suitable for predicting in-plane bending, out-of-plane bending and torsional behavior. Additionally, substudies were conducted to assess the influence on results of factors including centrifugal acceleration, Coriolis acceleration, and the structural effect of twist.

The resulting baseline single blade model consists of twenty CBAR elements and additions -- grid points, multipoint constraints, and plotting elements -- which permit "nice" plots of the undeformed structure, deformed structure, and mode shapes.

The baseline blade is twenty feet long, has a chord of 24 inches, weighs 370 pounds, has a uniform cross-section having properties summarized in Table I.

Birotor models were derived from the baseline model and consist of seventeen CBAR elements per blade for the 17' blade and fourteen CBAR elements per blade for the 14' blade. For both blade lengths additional CBAR elements are employed to model structural spacers.

The cross-sections, again uniform, have properties summarized in Table II.

The birotor blade lengths of seventeen feet (with a chord of 14.10 inches) and fourteen feet (with a chord of 16.98 inches) were selected to provide a composite lift equal to that of the baseline blade for the same tip speed (600 ft/sec). Composite lift, as will be noted in a subsequent section, worked out to be roughly twenty-five percent higher than that of the baseline blade for the 17' birotor, and roughly equal to that of the baseline blade for the 14' birotor.

Individual birotor blade weight was set equal to 185 pounds to provide a total weight equal to that of the baseline blade. This decision was somewhat arbitrary and should not be interpreted to imply that a birotor system of lighter than baseline weight could not be constructed.

3. Local hub loads for the birotor are higher than those for the baseline single blade. As a consequence of non-zero stagger, the individual blade center of mass will be either forward or aft of the radial axis along which the blades will interface with the hub. Centrifugal loading, therefore, leads to transverse shear and in-plane bending stresses which must be reacted at the hub.
4. Although blade loads for the birotor are higher than for the baseline single blade, maximum blade stresses are similar, since the centrifugal loading described above is reacted by portions of the blade structure which are typically lightly loaded by aerodynamics.
5. Significant natural frequencies for the birotor configuration are generally in the range of significant natural frequencies for the baseline blade. The more complicated birotor structure leads to more modal activity in this range and significant coupling of in- and out-of-plane bending, and torsion.

In summary, although detailed blade and hub design were beyond the scope of the study, the work done leads the writer to conclude that, in spite of higher loads described above, the birotor concept is structurally feasible.

Some redesign of the blade structure may be required to efficiently react transverse shear and in-plane bending. The hub will, moreover, require additional structure to react birotor loads. Aerodynamic performance may be traded-off (by reducing blade stagger) to reduce loads and the consequent need for added structure.

The birotor concept is, additionally, attractive to the dynamicist since added latitude for tailoring natural frequencies and associated mode shapes is afforded by varying the location, stiffness, and end conditions of the structural spacers needed for a feasible birotor design.

Table I -- Properties for Baseline Blade

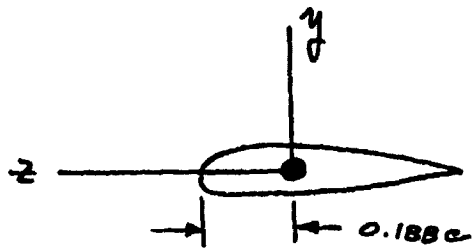

Material: Stainless, $E = 28 \times 10^6$, $G = 12.5 \times 10^6$ psi

Area : $5.39\ in^2$

I_{yy} : $93.89\ in^4$

I_{zz} : $4.63\ in^4$

I_{xx} : $18.94\ in^4$ *

* includes factor to account for warping of non-circular cross-sections.

Table II -- Properties for Birotor Blade

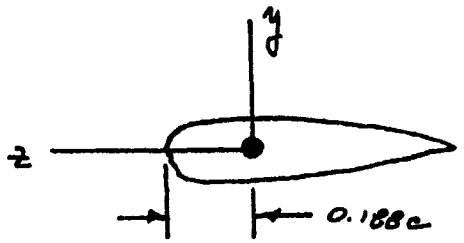

Material: Stainless, $E = 28 \times 10^6$, $G = 12.5 \times 10^6$ psi

17' birotor

Area : $3.19\ in^2$

I_{yy} : $19.06\ in^4$

I_{zz} : $0.941\ in^4$

I_{xx} : $3.84\ in^4$ *

14' birotor

Area : $2.70\ in^2$

I_{yy} : $23.53\ in^4$

I_{zz} : $1.16\ in^4$

I_{xx} : $4.746\ in^4$ *

*includes factor to account for warping of non-circular cross-sections.

Hover Loads

During the aerodynamic portion of this study, aerodynamic loads representing a steady-state hover condition were developed for the blades described in the previous section. These loads are given in Fig. 16 for the baseline blade, and are exemplified for a birotor (17' case) in Figs. 17 and Fig. 18.

The given aerodynamic loads were combined with gravity loading and centrifugal loading corresponding to a blade tip speed of 600 ft/sec. in order to develop the results described below.

Composite hub loads, i.e., loads due to a single baseline blade or to a pair of birotor blades are summarized in Table III. Six birotor cases were investigated.

The one-tie birotor cases incorporate a single structural spacer connecting the tips of the birotor blades. The two-tie birotor case incorporates a tip spacer and a spacer at roughly the second in-plane bending antinode. The multi-tie case incorporates a total of nine spacers positioned at every other model node point (approximately 2 feet apart).

The unique loading produced by birotor operation is represented in Table III by the torque directed along the blade, T_x. This is a gyroscopic torque developed as a consequence of the fact that the rotor spin axis is not parallel to a symmetry axis of a birotor blade pair. (The opposed blade pair produces an equal and opposite gyroscopic torque so that gyroscopics are reacted entirely within the hub assembly.)

The study requirement that birotor tip speed be equal to baseline blade tip speed leads to a higher spin rate for the birotor, and, therefore, to a proportionally higher birotor axial force, F_x.

The higher lift, F_y, seen for the 17' birotor leads as a consequence to a higher tangential torque, T_z. It is worth noting that this torque component increases less than proportionally with F_y when the 17' birotor and baseline blade are compared.

Worst case local hub loads, that is, worst case loads at a theoretical individual blade-hub interface, are summarized in Table IV. Clearly seen is the significant influence of spacers on the in-plane bending torque, T_y, and the out-of-plane bending torque, T_z.

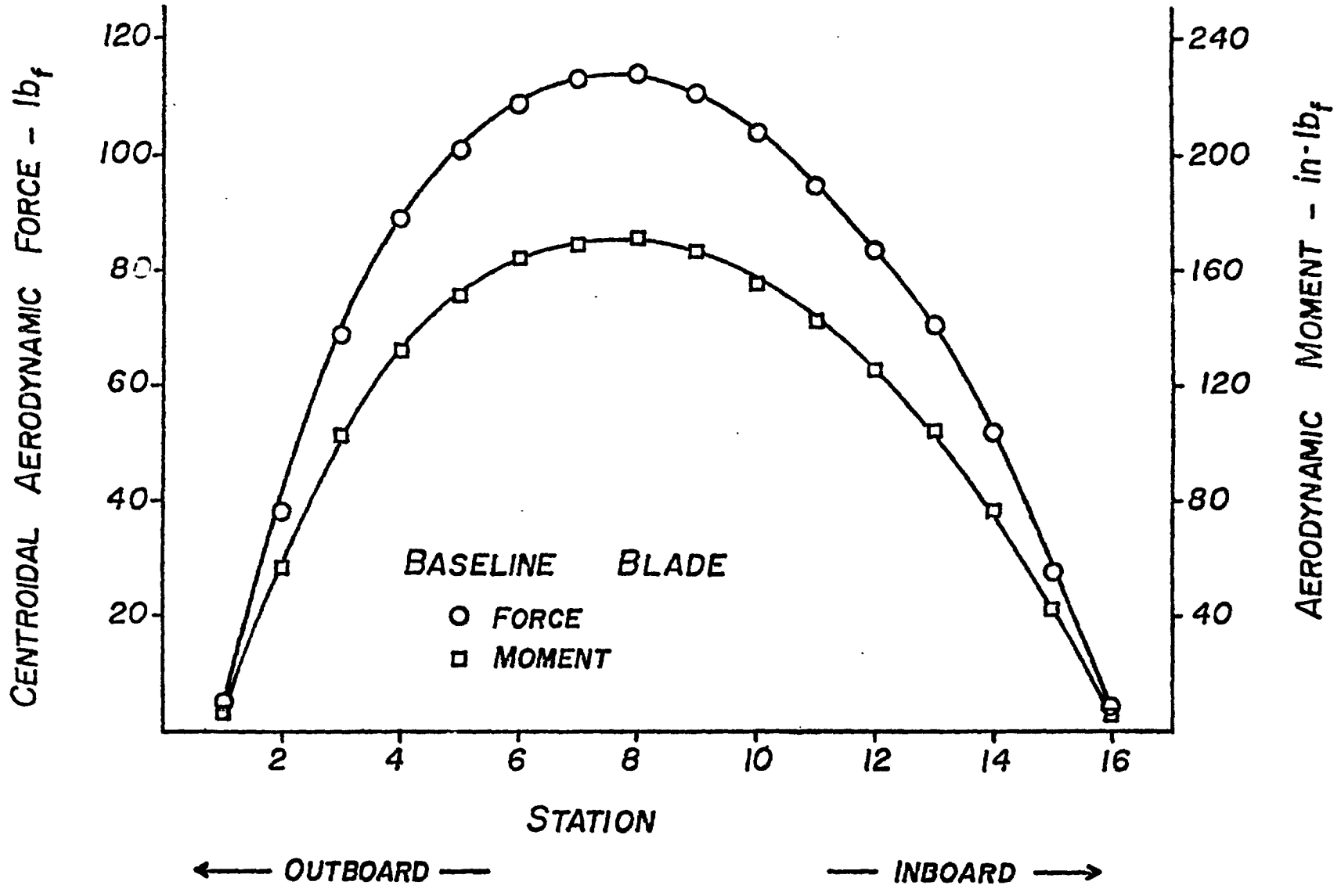
CENTROIDAL AERODYNAMIC FORCE - lb_f
AERODYNAMIC MOMENT - in-lb_f
120
100
80
60
40
20
240
200
160
120
80
40
BASELINE BLADE
FORCE
MOMENT
2
4
6
8
10
12
14
16
STATION
OUTBOARD
INBOARD

Figure 16

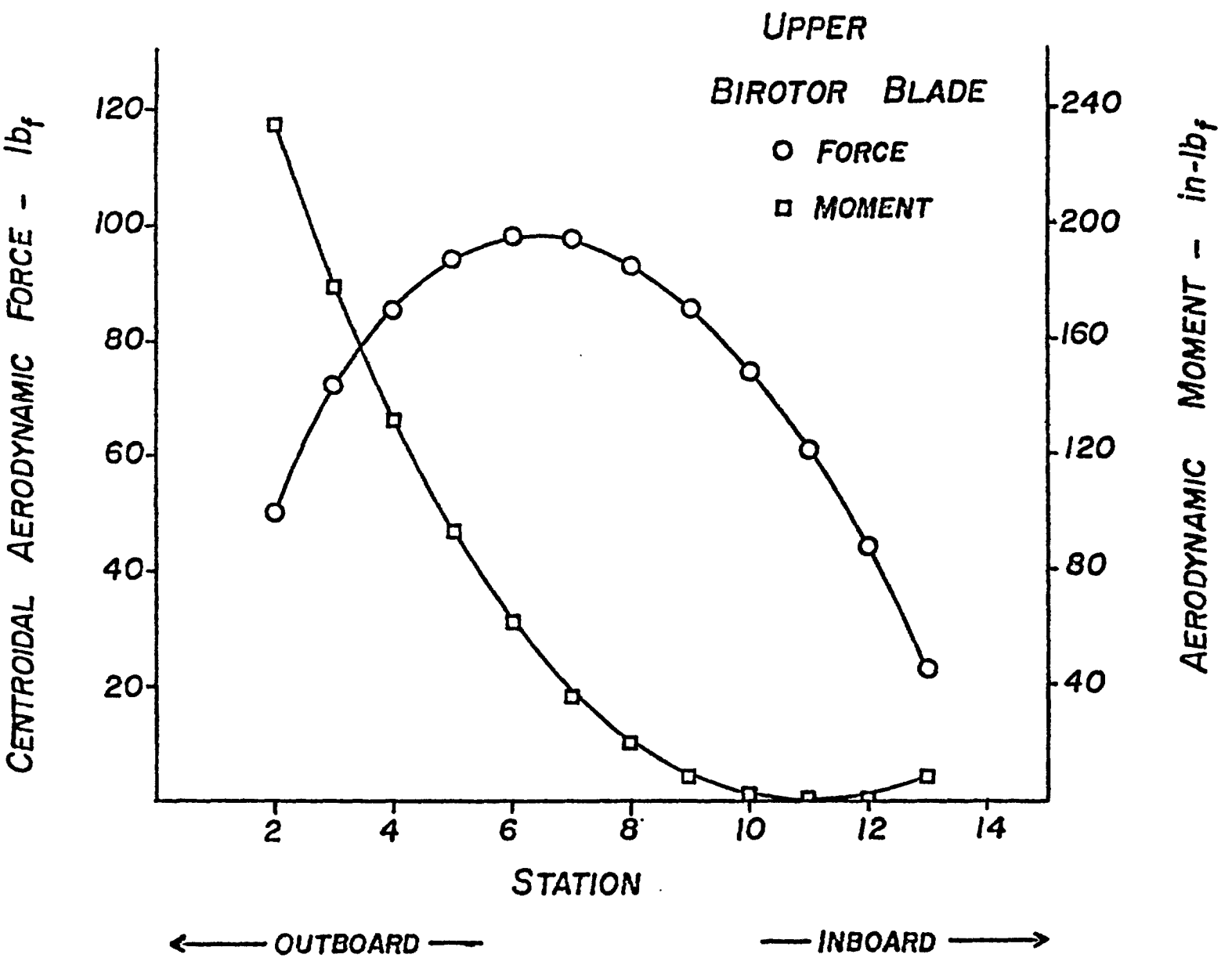
UPPER
BIROTOR BLADE
FORCE
MOMENT
CENTROIDAL AERODYNAMIC FORCE - lbf
AERODYNAMIC MOMENT - in-lbf
120
100
80
60
40
20
240
200
160
120
80
40
2
4
6
8
10
12
14
STATION
OUTBOARD
INBOARD

Figure 17

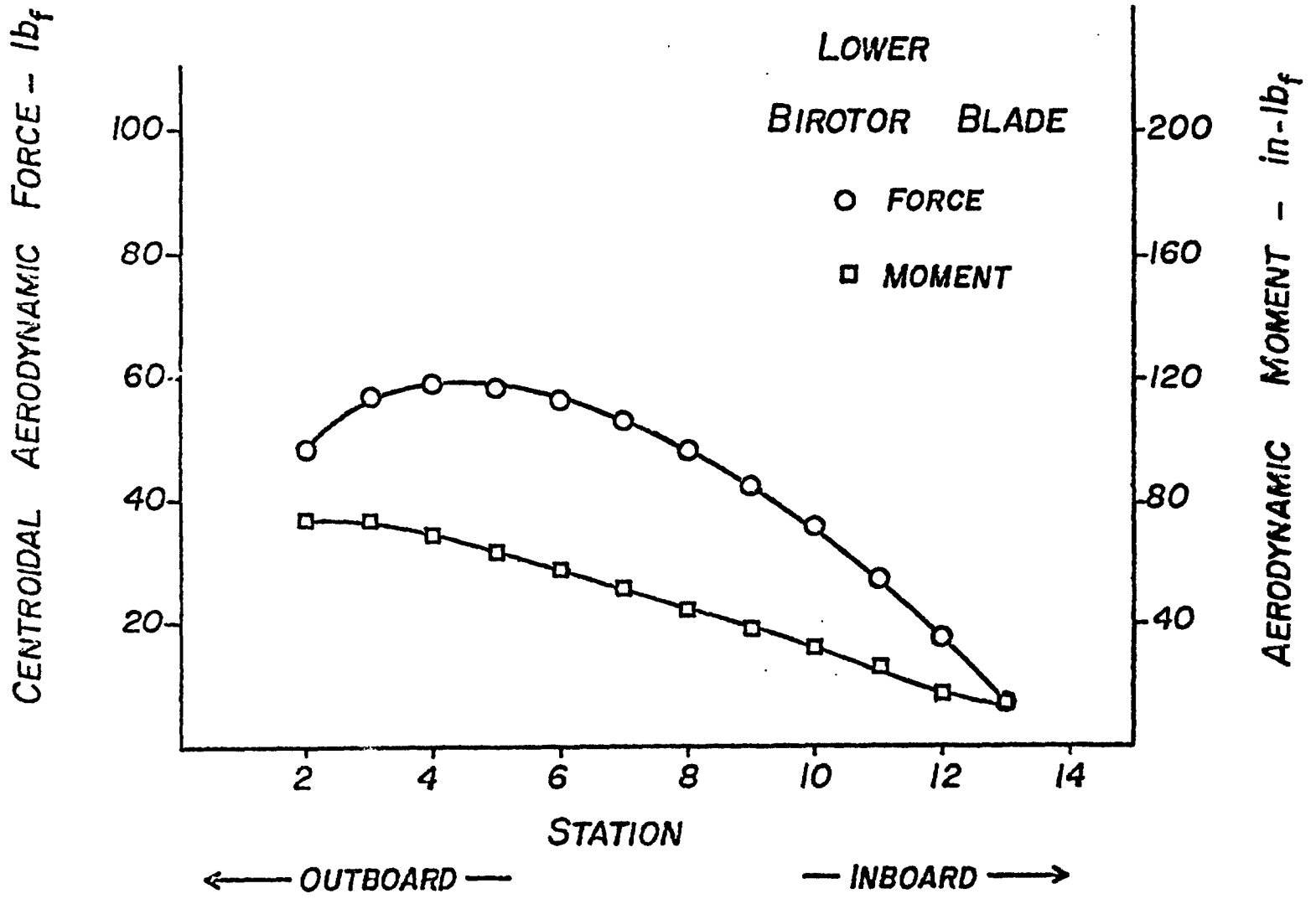
LOWER
BIROTOR BLADE
FORCE
MOMENT
CENTROIDAL AERODYNAMIC FORCE - lbf
AERODYNAMIC MOMENT - in-lbf
100
80
60
40
20
200
160
120
80
40
2
4
6
8
10
12
14
STATION
OUTBOARD
INBOARD

Figure 18

Table III -- Composite Hub Loads

Case	F_x	F_y	F_z	T_x	T_y	T_z
	(pounds)			(inch-pounds)		
Baseline	104000	810	0	1770	0	137000
All 17' cases	123000	1020	0	12700	0	149000
All 14' cases	146000	840	0	28800	0	105000

Table IV -- Worst Case Local Hub Loads

Case	F_x	F_y	F_z	T_x	T_y	T_z
	(pounds)			(inch-pounds)		
Baseline	104000	810	0	1770	0	137000
17' No tie	61000	690	$\pm$4200	-770	$\pm$432000	96700
17' One tie	64000	600	$\pm$2600	2600	$\begin{pmatrix}127000\\-89000\end{pmatrix}$	74600
17' Two tie	66000	540	$\pm$1800	3700	83000	67500
17' Nine tie	71000	620	$\pm$ 650	4500	83000	58100
14' No tie	73000	580	$\pm$7200	-1020	$\pm$620000	69000
14' One tie	72000	500	$\pm$4500	5750	$\begin{pmatrix}166000\\149000\end{pmatrix}$	53000

The spacers are also seen to produce with increasing number a reduction in tangential shear, F_z and an increase in radially directed torque, T_x.

In Table V are summarized, for the several birotor configurations, worst case deflections of one birotor blade with respect to the other. Inspection of this table reveals why structural spacers are required. The change in gap for the "untied" 17' blades, for example, is roughly four times the intended gap and the change in stagger is roughly equal to the intended stagger. Aerodynamics will be severely influenced and blade impacting seems a certainty. The single spacer case produces a worst case change in gap of approximately 20% of gap for the 17' case and 14% of gap for the 14' case. These configurations are acceptable structurally and may be acceptable aerodynamically. The 17' two spacer configuration appears fully acceptable from both standpoints and additional spacers offer no great advantage.

Worst case blade stresses are exemplified in Table VI for the 17' case. These stresses were developed for the cross-section properties illustrated in Tables I and II and are presented for comparative purposes only. Calculations are given in the Appendix.

Worst case spacer loading is summarized in Table VII. Loading given for the 17' two spacer case was employed to size a spacer in order to assess the potential effects of spacers on birotor aerodynamics. The worst case normal stress will be approximately equal the sum of the stress due to bending

$$\sigma_1 = \frac{Mc}{I} \tag{1}$$

and the stress due to axial loading

$$\sigma_2 = \frac{P}{A} \tag{2}$$

For a uniform circular cross-section of radius r, eqs. (1) and (2) may be summed to yield

$$\sigma_n = \frac{M}{.7854\ r^3} + \frac{P}{3.1416\ r^2} \tag{3}$$

Given a working normal stress of 50 ksi, and Table VII values for M and P of 16900 inch-pounds and 2480 pounds respectively, eq. (3) may be written in r

Table V -- Worst Case Relative Deflection

Case	Δ Gap (inch)	Δ Stagger (inch)	Δ Twist (r)
17' No tie	17.6	16.7	0.004
17' One tie	0.733	0.728	0.002
17' Two tie	0.220	0.187	0.002
17' Nine tie	0.200	0.050	0.001
14' No tie	13.6	7.3	.001
14' One tie	0.633	0.190	.004

Table VI -- Worst Case Blade Stresses

Case	Normal Stress Bottom of Blade (ksi)	Normal Stress leading edge (ksi)
Baseline	61.9	~0.
17' No tie	100.	79.2
17' One tie	87.1	37.7
17' Two tie	81.4	32.2
17' Nine tie	74.5	33.8
14' No tie	87.6	111.2
14' One tie	73.2	49.2

Table VII -- Worst Case Spacer Loads

Case	Bending Moment (inch-pounds)		Shear (pounds)		Axial (pounds)	Torque (inch-pounds)
	plane 1	plane 2	plane 1	plane 2		
17' One tie	18300	2500	2700	310	1570	900
17' Two tie	16900	4600	2300	430	2480	220
17' Nine tie	10500	750	1400	100	500	170
14' One tie	5110	10300	600	1050	2660	520

$$r^3 - 0.01579\, r - 0.43035 = 0 \qquad (4)$$

The only real solution to eq. (4) is

$$r = 0.7620 \text{ inch}$$

It follows that the requisite spacer has a diameter of roughly an inch and a half.

Dynamics

Modal analysis was performed for the baseline configuration and for the six birotor configurations described in previous sections.

The modal behavior for the baseline blade is straightforward and is summarized in Table VIII.

Modal behavior for the 17' birotor configurations is summarized in Table IX. Modal behavior for the 14' birotor is not included since it exposes nothing new.

An examination of Tables VIII and IX illustrates that potentially significant birotor natural frequencies are not greatly different from corresponding baseline blade natural frequencies. Dynamic stability and control problems unique to the birotor concept will not be present, at least, based upon this preliminary view.

The additional complexity of birotor configurations suggests roughly a doubling of modes of vibration within the frequency band of interest. Roughly half of these modes depend strongly on the specifics of spacer design, location, and end conditions. None of these factors were investigated during the present study. Spacers, where employed, were assumed to be rigidly connected at individual blade centroids.

Spacers, moreover, modify symmetry of the blade configuration and tend, therefore, to couple in-plane bending, out-of-plane bending, and torsion.

The impact on helicopter flight stability and control of increased modal activity and modal coupling associated with the birotor configuration deserves further study.

Table VIII -- Baseline Simple Blade Modal Activity

Mode	Frequency(Hz)
Out-of-Plane Bending	
1st	1.74
2nd	10.9
3rd	30.4
In-Plane Bending	
1st	7.85
2nd	48.8
3rd	135.5
First Torsion	59.3

Table IX -- 17' Birotor Blade Modal Activity

Mode	Frequency(Hz)			
	No-tie	One-tie	Two-tie	Nine-tie
In-plane Bending				
1st	6.38	6.69	6.93	7.91
	(6.38)*	(27.5)	(coupled)	(coupled)
2nd	39.7	40.4	40.9	42.2
	(39.7)	(coupled)	(coupled)	(coupled)
3rd	111.0	111.2	111.3	112.8
	(111.0)	(coupled)	(coupled)	(coupled)
Out-of-Plane Bending				
1st	1.42	1.51	1.57	1.73
	(1.42)	(6.58)	(12.5)	(22.4)
2nd	8.85	9.08	9.27	9.70
	(8.85)	(19.4)	(24.3)	(53.9)
3rd	24.7	24.9	24.9	25.3
	(24.7)	(36.4)	(37.7)	(75.4)
First Torsion	69.7	87.2	100.8	141.2
	(69.7)	(coupled)	(coupled)	(coupled)

* Items in parentheses refer to a mode roughly corresponding, generally with blades out-of-phase.

Appendix

Stress Calculations

The text, Theory and Analysis of Flight Structures, provides the equation

$$\sigma_{xx} = \frac{P}{A} - \frac{M_z I_{yy} - M_y I_{yz}}{I_{yy} I_{zz} - I_{yz}^2}(y) - \frac{M_y I_{zz} - M_z I_{yz}}{I_{yy} I_{zz} - I_{yz}^2}(z) \qquad (1)$$

If twist is sufficiently small, $I_{yz} = 0$, and

$$\sigma_{xx} = \frac{P}{A} - \frac{M_z y}{I_{zz}} - \frac{M_y z}{I_{yy}} \qquad (2)$$

where

P : axial load

M_y: torque about an axis perpendicular to the chord intersecting the elastic axis

M_z: torque about an axis parallel to the chord intersecting the elastic axis

and where I_{yy} and I_{zz} are accordingly defined.

Sample Calculation

For the 17' birotor with one tie, Table IV gives

$F_x = P = 64000$ pounds

$T_y = M_y = 127000$ inch-pounds

$T_z = M_z = 74600$ inch-pounds

Table II gives

Area = $A = 3.19$ inch^2

$I_{yy} = 19.06$ inch^4

$I_{zz} = 0.941$ inch^4

On the bottom of the blade y = -1.44 inch (1.44 = .12 x 14.10/2), z = 0, and

$$\sigma_{xx} = \frac{64000}{3.19} + \frac{74600(1.44)}{.941}$$

$$\sigma_{xx} = 87.1 \text{ ksi}$$

At the leading edge of the blade of y = 0, and z = 2.65 inches (.188 x 14.10), and

$$\sigma_{xx} = \frac{64000}{3.19} + \frac{127000(2.65)}{19.06}$$

$$\sigma_{xx} = 37.7 \text{ ksi}$$

REFERENCES

1. Nenadovitch, M., "Recherches sur les Cellules Biplane Rigides d'Enverqure Infine," Publications Scientifiques et Techniques du Minister de L'Air, Institut Aerotechnique de Saint-Cyr, Paris, 1936.

2. Raj, P. and Gray, R. B., "Computation of Two-Dimensional Potential Flow Using Elementary Vortex Distribution," Journal of Aircraft, Vol. 15, October 1978, pp. 698-700.

3.,4. Kreuler, R. J., and Gregorek, G. M., "An Evaluation of Four Single Element Air-foil Analytic Methods," General Aviation Design and Analysis Center, The Ohio State University.

5. Truckenbrodt, E., "A Method of Quadrature for Calculation of the Laminar and Turbulent Boundary Layer in Case of Plane and Rotationally Symmetric Flow," NACA TM-1379, 1955.